Global Attitude Estimation and Dead Reckoning of a Spherical Robot Using Extended Kalman Filter

A Project Report

submitted by

VANJPE OMKAR KALIDAS (EE13B131)

in partial fulfilment of requirements
for the award of the dual degree of

BACHELOR OF TECHNOLOGY AND MASTER OF TECHNOLOGY

DEPARTMENT OF ELECTRICAL ENGINEERING
INDIAN INSTITUTE OF TECHNOLOGY MADRAS

MAY 2018

THESIS CERTIFICATE

This is to certify that the thesis titled **Global Attitude Estimation and Dead Reckoning of a Spherical Robot Using Extended Kalman Filter**, submitted by **Vanjpe Omkar Kalidas, EE13B131**, to the Indian Institute of Technology Madras, for the award of the dual degree of **Bachelor of Technology and Master of Technology**, is a bona fide record of the research work done by him under our supervision. The contents of this thesis, in full or in parts, have not been submitted to any other Institute or University for the award of any degree or diploma.

Dr. Arun Mahindrakar
Research Guide
Associate Professor
Dept. of Electrical Engineering
IIT Madras, 600036

Date: 21st May 2018

Place: Chennai

ACKNOWLEDGEMENTS

I would like to take this opportunity express my sincere gratitude to my guide Dr. Arun Mahindrakar for his encouragement and timely guidance. I thank him for the opportunity he has given me to explore robotics from a research perspective that has kindled my interest further.

I would also like to thank Mundla Narsimhappa for his invaluable help, constant support and mentoring throughout the project. I thank him for his technical help whenever I struggled.

I would also like to thank Akshit Saradagi for being approachable and ready to help at all times.

A special thanks to my friends and wing mates for adding great fun and making my life in the institute a memory to be cherished for a lifetime.

Finally I would like to thank my parents for supporting me in all my endeavors and being there me in the toughest of times and making me into who I am today.

ABSTRACT

KEYWORDS: Spherical Robot, Attitude Estimation, Quaternion, Extended Kalman Filter

This project explores a stochastic approach to estimate the attitude of a spherical robotic system. It takes the noise corrupted data from inertial measurement unit (IMU) and uses a quaternion based extended Kalman filter algorithm to give the pose estimate of the robot. Using the nonholonomic constraints of the robot and no-slip condition, the trajectory is calculated, and then compared with the truth. Robustness analysis is done using the comparison of body angular velocities and Euler angles. The algorithm is tested on a real-world spherical robot system by dead-reckoning on circular and trifolium trajectory, and the results are compared and analyzed.

TABLE OF CONTENTS

LIST OF FIGURES

ABBREVIATIONS

IITM	Indian Institute of Technology Madras
EKF	Extended Kalman Filter
AHRS	Attitude Heading Reference System
UAV	Unmanned Aerial Vehicle
RMSE	Root Mean Squared Error

NOTATION

r	Radius, m
a	Linear acceleration in inertial frame, m/s^2, $a \in \mathbb{R}^3$
ω	Body angular velocity, rad/s, $\omega \in \mathbb{R}^3$
m	Magnetic field in inertial frame, T, $m \in \mathbb{R}^3$
Ω	Spacial angular velocity, rad/s, $\Omega \in \mathbb{R}^3$
$\hat{\omega}$	Skew symmetric matrix corresponding to body angular velocity, $\hat{\omega} \in \mathsf{so}(3)$
R	Rotation matrix, $R \in \mathrm{SO}(3)$
ψ**,**θ**,**ϕ	Yaw, pitch and roll respectively, rad

CHAPTER 1

INTRODUCTION

1.1 Background

The development and control of a spherical shaped robot has been an interesting research topic over the last two decades. One of the biggest advantage spherical robots have over other wheeled mechanisms is the omnidirectional mobility they provide. Many novel designs based on various techniques have been generated (Bhattacharya and Agrawal, 2000). Some of them use a wheeled robot to displace the barycenter. Some others use internally driven pendulum which imparts torque on outer shell.

This paper considers an internal rotor driven mechanism which produces reaction torque on spherical shell when actuated (Morinaga *et al.*, 2014). This system has non-holonomic constraints, which makes it difficult to model and control (Urakubo *et al.*, 2016).

The attitude and the orientation estimation is a crucial precursor step to all the navigation and control algorithms especially used in aerial robotics in recent times (Jing *et al.*, 2017) (Leccadito *et al.*, 2015). The attitude can be represented in three forms namely Euler angles, direction cosine matrices (DCM) and quaternions. While direction cosine matrices need larger storage due to 9 elements, euler angles suffer from a singularity known as "gimbal lock" problem where one degree-of-freedom is lost at a specific orientation. Quaternions need only 4 elements to store and do not suffer from singularity faced by Euler angles. Thus, it is the preferred choice (Diebel, 2006).

With the advent of MEMS technology, there has been an exponential rise in the use of compact, low-cost inertial measurement units (IMUs) for this purpose. Accelerometer in these sensors cannot detect rotation about the vertical axis. Therefore, often these inertial sensors are used in combination with magnetic, vision based systems. Some popular deterministic algorithms such as TRIAD and QUEST have been developed to fuse the sensor outputs. The measurements obtained are often prone to environmental

noise. In such cases, a deterministic approach to estimation may not be a good choice (Kok *et al.*, 2017). Extended Kalman filter is a stochastic algorithm which is practically used in many applications (Lefferts *et al.*, 1982).

1.2 Organization

The paper is organized as follows. Section II discusses the preliminaries of attitude estimation that are required. Section III gives description of the spherical robot kinematics and the sensor outputs. Kalman filter and its nonlinear extension is discussed in section IV. Finally, section V gives experimental results and analysis. Section VI concludes the paper.

CHAPTER 2

ATTITUDE ESTIMATION

The quaternion can be represented as follows

$$q = [q_0 q_1 q_2 q_3]^\top = [q_0 q_v]^\top \tag{2.1}$$

where q_0 is the scalar part and $q_v = (q_1, q_2, q_3)$ is the vector part.

The time derivative of the quaternion is computed by the following identity

$$\dot{q} = \frac{1}{2}\Omega(\omega)q \tag{2.2}$$

where $\boldsymbol{\omega} = (\omega_x, \omega_y, \omega_z) \in \mathbb{R}^3$ are the angular rates and $G(\omega)$ is defined as:

$$G(\omega) = \begin{bmatrix} 0 & -\omega^\top \\ \omega & -\hat{\omega} \end{bmatrix} \tag{2.3}$$

Here, $\hat{\omega}$ is the skew symmetric operator defined as

$$\hat{\omega} = \begin{bmatrix} 0 & -\omega_3 & \omega_2 \\ \omega_3 & 0 & -\omega_1 \\ -\omega_2 & \omega_1 & 0 \end{bmatrix} \tag{2.4}$$

The rotations from a vector x^b in body coordinate frame to a vector x^i inertial coordinate frame can be represented as $x^b = C_i^b(q)x^i$, where assuming $|q| = 1$, $C_i^b(q)$ is described as (Diebel, 2006)

$$C_i^b(q) = \begin{bmatrix} q_0^2 + q_1^2 - q_2^2 - q_3^2 & 2(q_1q_2 + q_0q_3) & 2(q_1q_3 - q_0q_2) \\ 2(q_1q_2 - q_0q_3) & q_0^2 - q_1^2 + q_2^2 - q_3^2 & 2(q_0q_1 + q_2q_3) \\ 2(q_1q_3 + q_0q_2) & 2(q_2q_3 - q_0q_1) & q_0^2 - q_1^2 - q_2^2 + q_3^2 \end{bmatrix} \tag{2.5}$$

The Euler angles corresponding to ZYX convention, also known as $yaw(\psi)$, $pitch(\theta)$

and $roll(\phi)$ can be estimated as (Murray, 2017)

$$\begin{bmatrix} \phi_{est} \\ \theta_{est} \\ \psi_{est} \end{bmatrix} = \begin{bmatrix} \arctan\left(\frac{2(q_2q_3+q_0q_1)}{\left(q_3^2+q_0^2-q_1^2-q_2^2\right)}\right) \\ -\arcsin\left(2\left(q_1q_3-q_0q_2\right)\right) \\ \arctan\left(\frac{2(q_1q_2+q_0q_3)}{\left(q_0^2+q_1^2-q_2^2-q_3^2\right)}\right) \end{bmatrix}. \tag{2.6}$$

CHAPTER 3

SYSTEM MODELLING

3.1 Kinematics of the spherical robot

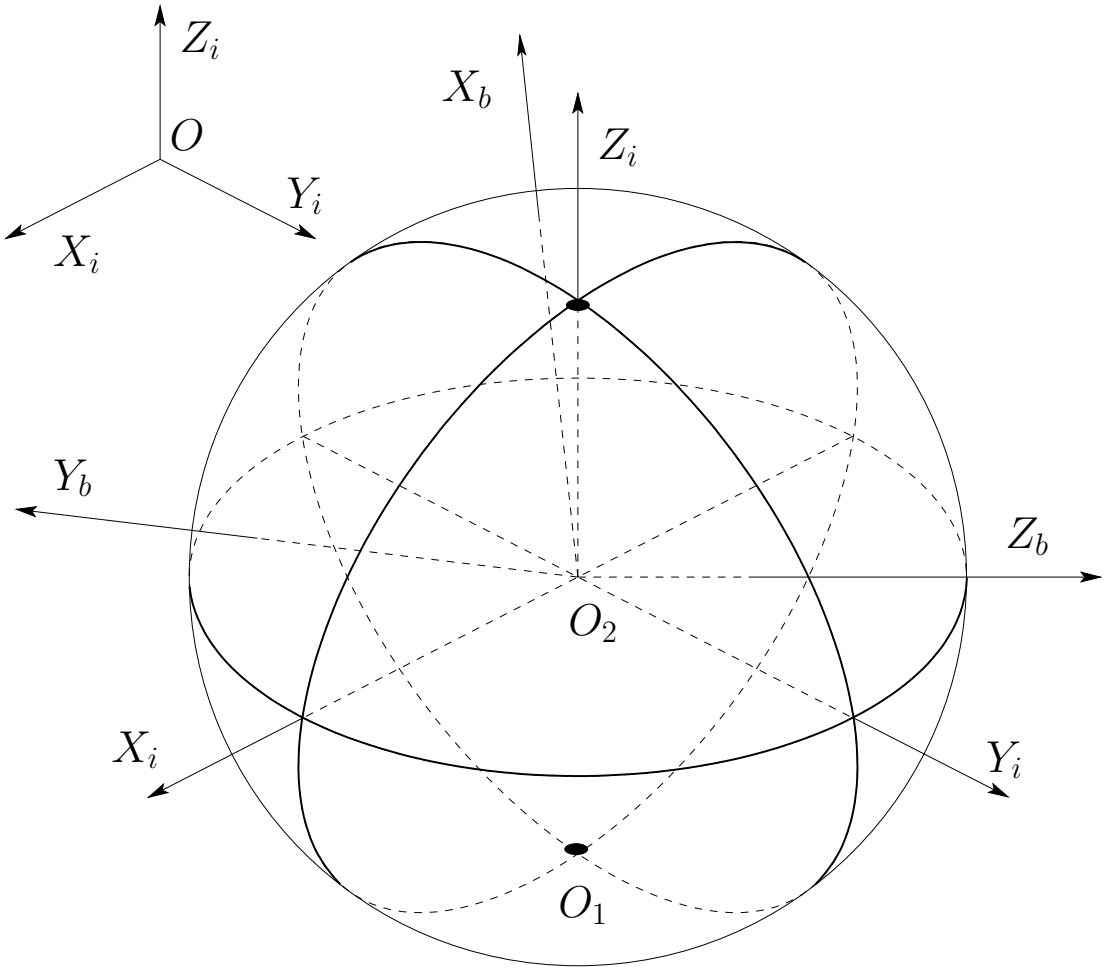

Figure 3.1: Schematic of the spherical robot

The spherical robot schematic shown in Figure 3.1 consists of a spherical shell of mass m and radius r moving in a horizontal plane. The center-of-mass of the robot is assumed to coincide with the geometric center. The position coordinates of the point O_1 with respect to O are denoted by (x, y). The orientation of body frame (X_b, Y_b, Z_b) of the robot with respect to an inertial frame (X_i, Y_i, Z_i) is given by a rotation matrix $R \in \mathrm{SO}(3)$. The robot has three independently controlled rotors with inertia wheels

along the body axes. Thus, three independent torques acting about the axes of the body-coordinate frame are generated. The rotor angles are denoted by ψ_1, ψ_2 and ψ_3.

The configuration space is $Q = \mathbb{R}^2 \times \mathrm{SO}(3) \times (S^1 \times S^1 \times S^1)$, parameterized by $\bar{q} = (x, y, R, \psi_1, \psi_2, \psi_3) \in Q$. The rotor positions are of no interest while proceeding with the kinematics and thus the motion of the spherical robot can be conveniently described by a curve $q(t) = (x(t), y(t), R(t)) \in \mathbb{R}^2 \times \mathrm{SO}(3)$, Thus, the configuration space is $Q = \mathbb{R}^2 \times \mathrm{SO}(3)$ and $TQ = Q \times \mathbb{R}^2 \times \mathrm{so}(3)$.

The spherical robot is subjected to no-slip constraints given by

$$v = \begin{bmatrix} \dot{x} \\ \dot{y} \\ \dot{z} \end{bmatrix} = \Omega \times \begin{bmatrix} 0 \\ 0 \\ r \end{bmatrix} = r\ R\omega \times e_3, \tag{3.1}$$

where, $\omega \in \mathbb{R}^3$ denotes the body angular velocity and $\Omega \in \mathbb{R}^3$ is the spatial angular velocity of the robot.

The kinematics of the spherical robot is given by

$$\begin{aligned} \dot{x} &= r(\omega \cdot r_2) \\ \dot{y} &= -r(\omega \cdot r_1) \\ \dot{R} &= R\widehat{\omega}. \end{aligned} \tag{3.2}$$

where the rows of the rotation matrix R are denoted by by r_1, r_2, r_3. Here, $R = C_b^i = {C_i^b}^\top$.

3.2 Sensor model

The IMU consisting of accelerometer, gyroscope and magnetometer is mounted at the center of the spherical robot to give raw measurements. The gyroscope measures angular rates $(\omega_x, \omega_y, \omega_z)$ with respect to body frame. The accelerometer and magnetometer respectively measure the linear acceleration (a_x, a_y, a_z) and magnetic field vector (m_x, m_y, m_z) in inertial frame. The sensor readings are assumed to have a constant biases $b = (b_a, b_g, b_m)$ and to be corrupted by independent white Gaussian noise

$\eta = (\eta_a, \eta_g, \eta_m)$ with zero mean and variances $\sigma = (\sigma_a^2, \sigma_g^2, \sigma_m^2)$ for accelerometer, gyroscope and magnetometer respectively. Thus, the 9-DOF sensor model is described by

$$a_{meas} = R(q)^\top a_{true} + b_a + \eta_a \tag{3.3}$$

$$\omega_{meas} = \omega_{true} + b_g + \eta_g \tag{3.4}$$

$$m_{meas} = R(q)^\top m_{true} + b_m + \eta_m \tag{3.5}$$

From accelerometer and magnetometer data components, Euler angles can be obtained as follows (Ozyagcilar, 2012)

$$\begin{bmatrix} \phi_{meas} \\ \theta_{meas} \\ \psi_{meas} \end{bmatrix} = \begin{bmatrix} \arctan(-a_y/a_z) \\ \arcsin(-a_x/\sqrt{a_x^2 + a_y^2 + a_z^2}) \\ \gamma \end{bmatrix}. \tag{3.6}$$

CHAPTER 4

EXTENDED KALMAN FILTER

4.1 Kalman filter model

For a linear dynamical system, the state and measurement equations can be written as:

$$\mathbf{x_k} = \mathbf{F}\mathbf{x_{k-1}} + \mathbf{w_{k-1}} \tag{4.1}$$

$$\mathbf{z_k} = \mathbf{H}\mathbf{x_k} + \mathbf{v_k} \tag{4.2}$$

where $\mathbf{x_k} \in \mathbb{R}^{\mathbf{n}}$ and $\mathbf{F} \in \mathbb{R}^{\mathbf{n}\times\mathbf{n}}$ are the state vector and state transition matrix at epoch k respectively; $\mathbf{w_{k-1}}$ is the system noise; $\mathbf{z_k}$ is the observation at epoch k; $\mathbf{H}$ represents the observation matrix and v_k is the measurement noise. It is assumed that the process and measurement noises $\mathbf{w_{k-1}}$, $\mathbf{v_k}$ have a white Gaussian distribution and are statistically independent from each other.

The state vector consists of the attitude quaternion, accelerometer biases and magnetometer biases.

$$\mathbf{x_k} = (q(k),\ b_a(k),\ b_m(k)) \in \mathbb{R}^{10} \tag{4.3}$$

The quaternion update equation 2.2 is nonlinear. It can be linearized by taking first order Taylor series expansion.

$$\mathbf{f_k} = \mathbf{I_{4\times4}} + \frac{1}{2}\Omega(\tilde{\omega_k})T_s \tag{4.4}$$

where $\tilde{\boldsymbol{\omega}_k} \in \mathbb{R}^3$ is the bias corrected gyroscope vector. $\tilde{\boldsymbol{\omega}_k} = (\omega_1, \omega_2, \omega_3) - (b_{gx}, b_{gy}, b_{gz})$. T_s is the time interval between consecutive epochs.

The assumption of constant biases gives

$$\begin{bmatrix} b_a(k) \\ b_m(k) \end{bmatrix} = \begin{bmatrix} b_a(k-1) \\ b_m(k-1) \end{bmatrix} \tag{4.5}$$

Thus, the state space equation (4.1) can be rewritten as

$$\begin{aligned}\mathbf{x_k} &= \mathbf{F}\mathbf{x_{k-1}} + \mathbf{w_{k-1}} \\ &= \begin{bmatrix} \mathbf{f_k} & 0 & 0 \\ 0 & I & 0 \\ 0 & 0 & I \end{bmatrix} \mathbf{x_{k-1}} + \mathbf{w_{k-1}}\end{aligned} \tag{4.6}$$

The process noise in quaternion components and bias in all the dimensions is assumed to be independent of each other. Further, the quaternion noise can be taken as(Sabatini, 2006),

$$\Xi(k) = -\frac{T_s}{2}\begin{bmatrix} q_0(k)I + [q_v(k)\times] \\ q_v(k) \end{bmatrix} \tag{4.7}$$

This gives

$$\mathbf{Q_k} = \begin{bmatrix} (T_s/2)^2\Xi(k)\sigma_g(k)^2\Xi(k)^T & 0 & 0 \\ 0 & T_s\sigma_a^2 I & 0 \\ 0 & 0 & T_s\sigma_m^2 I \end{bmatrix} \tag{4.8}$$

The measurement vector includes accelerometer and magnetometer readings at each epoch. The reference acceleration a_0 and magnetic field vector m_0 in the inertial frame is taken as

$$a_0 = (0, 0, 1)$$
$$m_0 = (m_x, 0, m_z)$$

From (3.3) and (3.5) the acceleration and magnetic field vectors in body frame can be

$$\mathbf{H_k} = \begin{bmatrix} -2q_2 & 2q_3 & -2q_0 & 2q_1 & 0 & 0 & 0 \\ 2q_1 & 2q_0 & 2q_3 & 2q_2 & 0 & 0 & 0 \\ 0 & -4q_1 & -4q_2 & 0 & 0 & 0 & 0 \\ -2m_z q_2 & 2m_z q_3 & -4m_x q_2 - 2m_z q_0 & -4m_x q_3 + 2m_z q_1 & 0 & 0 & 0 \\ -2m_x q_3 + 2m_z q_1 & 2m_x q_2 + 2m_z q_0 & 2m_x q_1 + 2m_z q_3 & -2m_x q_0 + 2m_z q_2 & 0 & 0 & 0 \\ 2m_x q_2 & 2m_x q_3 - 4m_z q_1 & 2m_x q_0 - 4m_z q_2 & 2m_x q_1 & 0 & 0 & 0 \end{bmatrix} \tag{4.10}$$

calculated at any epoch k as

$$\begin{aligned} a(k) = C_i^b(q(k))a_0 &= \begin{bmatrix} 2(q_1q_3 - q_0q_2) \\ 2(q_0q_1 + q_2q_3) \\ q_0^2 - q_1^2 - q_2^2 + q_3^2 \end{bmatrix} \\ m(k) = C_i^b(q(k))m_0 & \\ &= \begin{bmatrix} m_x(q_0^2 + q_1^2 - q_2^2 - q_3^2) + 2m_z(q_1q_3 - q_0q_2) \\ 2m_x(q_1q_2 - q_0q_3) + 2m_z(q_0q_1 + q_2q_3) \\ 2m_x(q_1q_3 + q_0q_2) + m_z(q_0^2 - q_1^2 - q_2^2 + q_3^2) \end{bmatrix} \end{aligned} \tag{4.9}$$

The Jacobian of (4.9) with respect to $\mathbf{x_k}$, denoted by $\mathbf{H_k}$ is shown in (4.10).

This $\mathbf{H_k}$ can be used as observation matrix in state equation (4.2).

The measurement noise in all the directions of accelerometer and magnetometer data is assumed to be statistically independent of each other. Thus, noise covariance matrix can be taken as (Sabatini, 2006)

$$\mathbf{R_k} = \begin{bmatrix} \sigma_a^2 I & 0 \\ 0 & \sigma_m^2 I \end{bmatrix} \tag{4.11}$$

4.2 Extended Kalman Filter algorithm

Extended Kalman filter is a two-step iterative stochastic algorithm which gives state and error covariance at each epoch. It first predicts the state apriori based on system model and then corrects the estimate based on actual observations. The initial state and error covariance matrix of the state are assumed to be $\hat{\mathbf{x}}_\mathbf{0}$ and $\hat{\mathbf{P}}_\mathbf{0}$ respectively while $\mathbf{K_k}$ is the Kalman gain. $\mathbf{Q_k}$ and $\mathbf{R_k}$ are the process noise covariance matrix and measurement noise covariance matrix respectively.

The two step iterative filtering algorithm is as follows

4.2.1 Prediction step

An apriori estimate based on state transition function $\mathbf{F_{k-1}}$ and previous state $\mathbf{x_{k-1}}$ is calculated.

$$\mathbf{\hat{x}_{k|k-1}} = \mathbf{F_k}\mathbf{\hat{x}_{k-1|k-1}} \tag{4.12}$$

$$\mathbf{P_{k|k-1}} = \mathbf{F_k}\mathbf{P_{k-1|k-1}}\mathbf{F_k^T} + \mathbf{Q_k} \tag{4.13}$$

4.2.2 Update step

Based on the measurements $\mathbf{z_k} = [a(k), m(k)]$ and estimates $\mathbf{y_k}$ obtained from equations 4.9, error $\mathbf{e_k}$ is calculated and used for estimating aposteriori state.

$$\mathbf{v_k} = \mathbf{z_k} - \mathbf{y_k} \tag{4.14}$$

$$\mathbf{K_k} = \mathbf{P_{k|k-1}}\mathbf{H_k^T}(\mathbf{H_k}\mathbf{P_{k|k-1}}\mathbf{H_k^T} + \mathbf{R})^{-1} \tag{4.15}$$

$$\mathbf{\hat{x}_{k|k}} = \mathbf{\hat{x}_{k|k-1}} + \mathbf{K_k}\mathbf{v_k} \tag{4.16}$$

$$\mathbf{P_{k|k}} = \mathbf{P_{k|k-1}} - \mathbf{K_k}\mathbf{H_k}\mathbf{P_{k|k-1}} \tag{4.17}$$

CHAPTER 5

EXPERIMENTAL VALIDATION

5.1 Robot setup

The experimentation is performed on the spherical robot developed at the Dynamics and Control Laboratory, IIT Madras. The hardware consists of the dsPIC microcontroller with XBee wireless module for communication with remote PC. A digital nine degree-of-freedom IMU ADIS16400 is placed at the center of the spherical robot on a crossbeam attached to three orthogonal rings making up the endoskeleton. The entire setup is enclosed within a spherical acrylic shell made up of two detachable hemispheres that form the exoskeleton.

The robot is rolled without slipping on two paths - circular and trifolium with a goal of tracking the pose. Nonholonomic constraints mentioned in (3.2) are used to calculate the trajectory estimate.

Three figures of merit are chosen as follows:

1. Root mean square of the error in the estimated (x, y) position compared to true path.

2. Error in the estimated body angular velocity compared to measurements $|| \left(\boldsymbol{R}_{est}^T \dot{\boldsymbol{R}}_{est} \right)^\vee - \boldsymbol{\omega}_{meas} ||$, where $\vee$ is the inverse operator for the skew symmetric operator in (2.4).

3. Cross correlation between estimated output (x, y) and sampled values from true trajectory given by

$$x \star x_{true} = \frac{1}{N-1} \sum_{k=1}^{N} \frac{x\,[k]\, x_{true}\,[k]}{\sigma_x \sigma_{x_{true}}}$$

$$y \star y_{true} = \frac{1}{N-1} \sum_{k=1}^{N} \frac{y\,[k]\, y_{true}\,[k]}{\sigma_y \sigma_{y_{true}}}$$

where N is the total number of samples in the experiment.

Figure 5.1: Spherical Robot developed at IIT Madras

5.2 Magnetometer correction

Magnetometer data can be erroneous due to changes in the surrounding temperature, presence of hard and soft iron. These factors may produce a nonlinearity in the output which needs to be corrected. On rotating the setup about 360^0 about the inertial Z-axis the raw X and Y data obtained is transformed to give the circle as shown in Figure 5.2. The magnetometer readings are modified as follows:

$$m_{x_{new}} = 0.9828 m_{x_{old}} + 1.450$$

$$m_{y_{new}} = m_{y_{old}} + 1.955$$

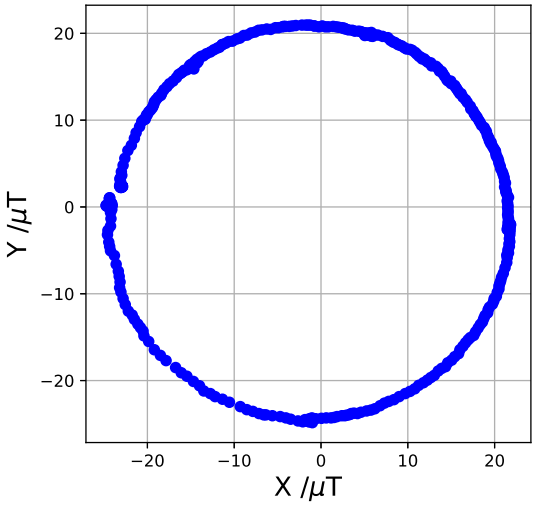

(a) Original magnetometer readings

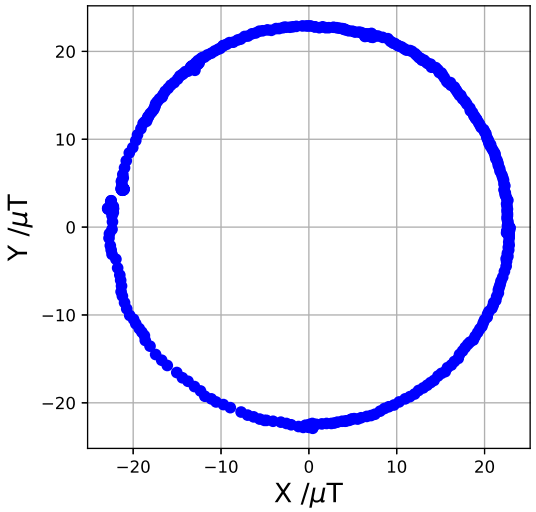

(b) Corrected magnetometer readings

Figure 5.2: Magnetometer correction

5.3 Results and analysis

The sampling frequency is 50Hz for both the experiments.

Other parameter details are as follows:

1. Initial quaternion is set as $q = [1,\ 0,\ 0,\ 0]$ along with following initial conditions -

$$Q\,(k) = 10^{-5} \times [I_{10\times 10}]$$

$$R\,(k) = 10 \times [I_{6\times 6}]$$

2. The initial alignment is such that magnetic field has components present only along x and z axes. Thus, normalized reference acceleration and magnetic field vectors are

$$a_0 = (0,\ 0,\ 1)$$
$$m_0 = (0.97,\ 0,\ 0.24)$$

5.3.1 Circle

For circular trajectory, the true trajectory is parametrized as follows

$$\begin{aligned} x_{true} &= r_c\left(1 - \cos\left(f_c t\right)\right) \\ y_{true} &= r_c \sin\left(f_c t\right) \end{aligned} \tag{5.1}$$

where $r_c = 1.25m$ is the radius of the desired circular trajectory and $f_c = \frac{2\pi}{N}$ for N sampling steps.

The results are shown in Figure 5.3 with initial condition as $(x, y) = (0, 0)$. Figure 5.3a shows that the Euler angles estimated by (2.6) and measured from raw data by (3.6) are close to each other. Figure 5.3b shows the norm of the error between estimated and measured angular velocity vector having a peak value of $0.5rad/s$. The estimated trajectory compared with the true trajectory is shown in Figure 5.3c. The cross correlation between estimated and true trajectory characterized by (5.1) is calculated to be $x \star x_{true} = 0.9973$ and $y \star y_{true} = 0.9978$ clearly indicating a strong match.

5.3.2 Trifolium

For trifolium trajectory, the true trajectory is parametrized as follows

$$\begin{aligned} x_{true} &= l_t \cos\left(3 f_c t\right) \sin\left(f_c t\right) \\ y_{true} &= l_t \cos\left(3 f_c t\right) \cos\left(f_c t\right) \end{aligned} \tag{5.2}$$

where $l_t = 2m$ is the petal length of the desired trifolium trajectory and $f_c = \frac{2\pi}{N}$ for N sampling steps.

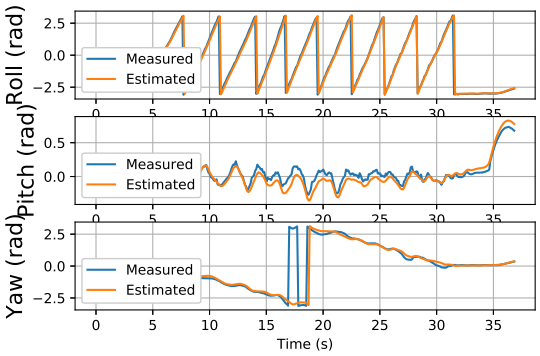

(a) Roll pitch yaw information of circular trajectory

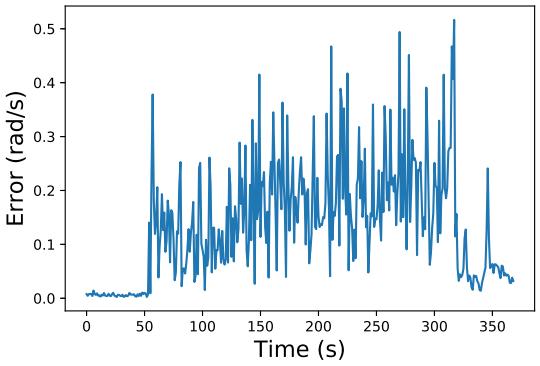

(b) Error between measured and estimated ω

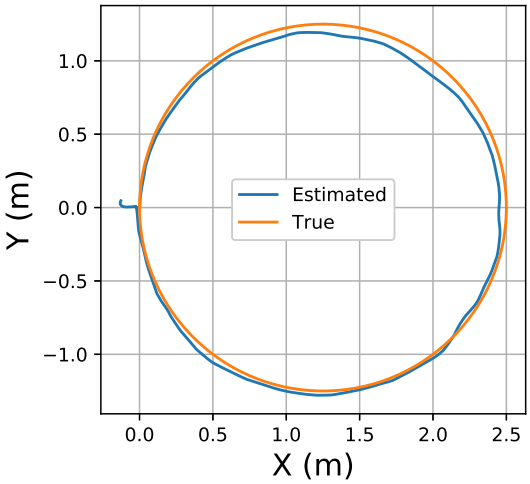

(c) Comparison of estimated and true trajectory

Figure 5.3: Results of dead reckoning about a circular trajectory

The results are shown in Figure 5.4 with initial condition as $(x, y) = (0, 0)$. Figure 5.4a shows that the Euler angles estimated by (2.6) and measured from raw data by (3.6) are close to each other. Figure 5.4b shows the norm of the error between estimated and measured angular velocity vector having a peak value of $0.8rad/s$. The estimated trajectory compared with the true trajectory is shown in Figure 5.4c. The cross corre-

lation between estimated and true trajectory characterized by (5.2) is calculated to be $x \star x_{true} = 0.9973$ and $y \star y_{true} = 0.9978$ clearly indicating a strong match.

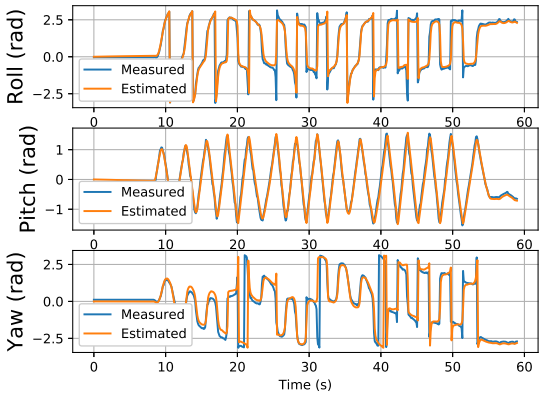

(a) Roll pitch yaw information of trifolium trajectory

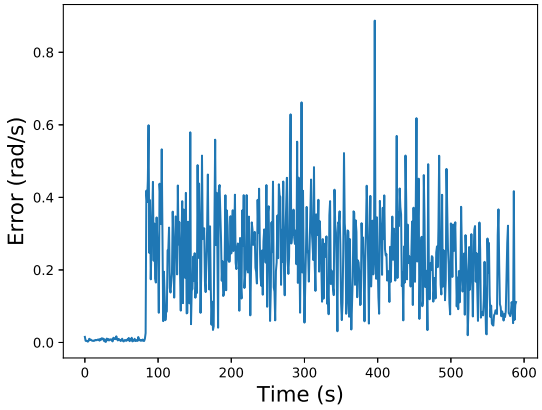

(b) Error between measured and estimated ω

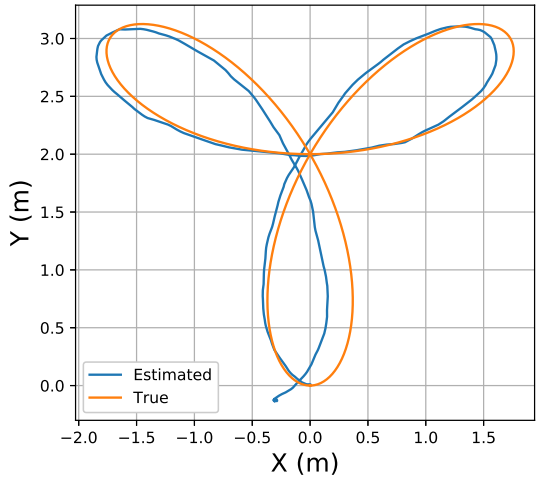

(c) Comparison of estimated and true trajectory

Figure 5.4: Results of dead reckoning about a trifolium trajectory

CHAPTER 6

CONCLUSION AND FUTURE WORK

6.1 Summary

The thesis introduces quaternion based extended Kalman filter to estimate the global attitude of a spherical robot system. The data obtained from inertial measurement unit (IMU) is subjected to iterative filtering which produces the trajectory information. The robustness of this algorithm is checked by incorporating three figure of merits - RMSE of coordinates, error in body angular velocity, and cross-correlation with true trajectory. The results are plotted after rolling on circular and trifolium path and closeness with true values is observed.

6.2 Future work

Solving the nonholonomic constraints for control of the robot using the attitude information derived from EKF is the next step. Intelligent control methods like reinforcement learning can also be explored.

REFERENCES

1. **Bhattacharya, S.** and **S. K. Agrawal** (2000). Spherical rolling robot: A design and motion planning studies. *IEEE Transactions on Robotics and Automation*, **16**(6), 835–839.

2. **Diebel, J.** (2006). Representing attitude: Euler angles, unit quaternions, and rotation vectors. *Matrix*, **58**(15-16), 1–35.

3. **Jing, X.**, **J. Cui**, **H. He**, **B. Zhang**, **D. Ding**, and **Y. Yang**, Attitude estimation for uav using extended kalman filter. *In Control And Decision Conference (CCDC), 2017 29th Chinese*. IEEE, 2017.

4. **Kok, M.**, **J. D. Hol**, and **T. B. Schön** (2017). Using inertial sensors for position and orientation estimation. *arXiv preprint arXiv:1704.06053*.

5. **Leccadito, M.**, **T. M. Bakker**, **R. Niu**, and **R. H. Klenke**, A kalman filter based attitude heading reference system using a low cost inertial measurement unit. *In AIAA Guidance, Navigation, and Control Conference*. 2015.

6. **Lefferts, E. J.**, **F. L. Markley**, and **M. D. Shuster** (1982). Kalman filtering for spacecraft attitude estimation. *Journal of Guidance, Control, and Dynamics*, **5**(5), 417–429.

7. **Morinaga, A.**, **M. Svinin**, and **M. Yamamoto** (2014). A motion planning strategy for a spherical rolling robot driven by two internal rotors. *IEEE Transactions on Robotics*, **30**(4), 993–1002.

8. **Murray, R. M.**, *A mathematical introduction to robotic manipulation*. CRC press, 2017.

9. **Ozyagcilar, T.** (2012). Implementing a tilt-compensated ecompass using accelerometer and magnetometer sensors. *Freescale semiconductor, AN*, **4248**.

10. **Sabatini, A. M.** (2006). Quaternion-based extended kalman filter for determining orientation by inertial and magnetic sensing. *IEEE Transactions on Biomedical Engineering*, **53**(7), 1346–1356.

11. **Urakubo, T.**, **M. Monno**, **S. Maekawa**, and **H. Tamaki** (2016). Dynamic modeling and controller design for a spherical rolling robot equipped with a gyro. *IEEE Transactions on Control Systems Technology*, **24**(5), 1669–1679.